REVISION 1

A New Method to Rapidly and Accurately Assess the Mechanical Properties of Geologically Relevant Materials

Pu Deng, Sean Vincent Herrera and Barton Charles Prorok*

Materials Research and Education Center, Auburn University, Auburn, AL USA

Abstract

A new indentation-based method was developed that will impact and facilitate the elastic property measurements of rocks and minerals, especially those possessing unusual deformation behavior including brittle materials and those with complex architectures. The novel feature employed is a metallic film that uniformly transfers the load from the indenter tip to the sample. The film also absorbs the damage caused by the penetrating indenter, shielding the material from highly localized deformation that can impact its response to loading. Many geologically relevant materials have resisted traditional indentation testing because they are either brittle in nature or possess highly anisotropic architectures, such as layered or lamellar structures. In both cases, the highly localized deformation from direct indentation significantly affects the indenter unloading stiffness, from which the elastic properties are determined. The indirect indentation method developed here, demonstrated accurate determination of the elastic properties of many common geologic materials as well as materials that have resisted elastic characterization such as galena and talc.

* Corresponding Author (prorok@auburn.edu)

Introduction

The elastic properties of rocks and minerals have long been central to understanding and predicting the mechanical behavior of the Earth from a regional to a planetary scale. Recent decades have seen the development of many skillful techniques capable of measuring elastic properties, including their dependence on temperature and/or pressures relevant from the Earth's crust to its core. These include electromagnetic radiation (EMR), acoustic emission (AE), micro-seismic (MS), and many others, see (Angel et al., 2009) for a recent review. Given these significant advances, the accuracy of deformation models continues to depend on accurate property inputs, which should be reflective of the regional rocks and minerals relevant to the model. In this regard, the local environmental conditions that these materials form and exist in can influence their properties as a function of composition, structure, hydration, and other characteristics (Ersoy and Waller, 1995; Na et al., 2017; Raisanen, 2004; Sun et al., 2017; Tandon and Gupta, 2013). Thus, the mechanical behavior of many geologic relevant materials can vary appreciably from region to region (Atkinson, 1976; Blackman et al., 2002; King Hubbert, 1951; Meyers and Chawla, 2009; Riecker, 1984), warranting the need for simple, rapid and accurate tests to provide this information. Indentation has long been a popular technique to carry out elastic property measurements due to the minimal sample preparation and the rapid collection of numerous data points, important to robust statistical analyses (Oliver and Pharr, 1992; Oliver and Pharr, 2004). It also enables unrivaled spatial mapping of elastic properties to ascertain variations in sample composition, microstructure, and phases (Constantinides et al., 2006; Randall et al., 2009). An additional benefit is that indentation does not require specific expertise or access to special facilities and can be performed at most universities and research institutions. The basic premise involves pressing a sharp diamond tip of well-known geometry into the material while independently recording the load and indentation depth. The resistance to penetration is represented by

DOI: https://doi.org/10.2138/am-2021-7455. http://www.minsocam.org/

hardness (H) while the elastic behavior (E) is related to the slope of the unloading curve, the unloading stiffness (S), as in the following relations (Oliver and Pharr, 1992):

$$H = \frac{P}{a} \quad \text{and} \quad S = \frac{dP}{dh} = E\frac{2}{\sqrt{\pi}}\sqrt{a}\,, \qquad (1)$$

where p is the applied indenter load, a is the contact area between the indenter and sample, h is the indenter displacement into the sample surface and E is the elastic modulus of the sample. By oscillating the indenter tip during penetration, both properties can be monitored continuously as a function of depth, termed continuous stiffness (Pharr et al., 2009). The typical indentation test ranges from the nanometer to micron scale and can infer local variations in elastic behavior including; compositional and structural changes, different material phases, interfaces, and many other varying characteristics. (Hintsala et al., 2018).

The extraction of the elastic modulus from indentation can be problematic for materials that are brittle or that possess unusual deformation behavior (Chen et al., 2018; Pharr and Bolshakov, 2002), which many rocks and minerals do. For example, brittle materials that cannot plastically strain in response to indenter penetration instead generate cracks or other defects. These form during the loading cycle and dissipate energy through the creation of new surface. They have a significant effect on the unloading stiffness (S) as they consume stored elastic energy that would normally push back on the indenter as it is withdrawn. Thus, the extracted elastic modulus is measured to be lower than it actually is. Many geologic materials possess complex architectures whose deformation can alter the contact area with the indenter. For example, lamellar structured materials such as kyanite can deform by large-scale cleavage and sliding of layers relative to one another (Boland et al., 1977; Doukhan and Christie, 1982; Doukhan and Paquet, 1982; Lefebvre, 1982; Lefebvre and Menard, 1981; Mikowski et al., 2007; Mikowski et al., 2008; Raleigh, 1965). When indented, the layers themselves do not appreciably strain elastically or plastically. Instead, the sliding translates the concentrated indenter load a distance from the indent's normal area of influence. This wholescale layer sliding will then alter the contact area with the indenter tip, and therefore, the elastic pushback the material would exert when the tip is withdrawn. In other directions, the applied load can cause layers to separate, essentially creating surface and disrupting the transfer of load. In all of these cases, the extreme local deformation caused by the indenter penetration results in inelastic damage/deformation that affected the unloading stiffness and therefore, the extraction of the elastic response. There are many other geologic materials possessing complex architectures, silicates for example, which will encounter similar problems. The Indirect Indentation Method (IIM) can be employed to mitigate these issues (Chen et al., 2018). Here, the thin metallic film is deposited serves to absorb this inelastic damage while transferring the load to the material in a uniform manner. This enables the unloading stiffness to reflect the materials actual elastic properties.

The indirect indention method generates a film/substrate composite where both materials contribute to the loading and unloading response. It uses the Zhou-Prorok thin film indentation model to interpret and decouple the film/substrate composite response (Zhou and Prorok, 2010a; Zhou and Prorok, 2010b). This model leverages the King modified Doerner and Nix empirical function (Doerner and Nix, 1986; King, 1987), which is rearranged into the basic form of the inverse rule of mixtures with elastic compliance (Reuss, 1929), see Equation 2. Here, E is the elastic modulus obtained from the indenter, E_f and E_s are the elastic moduli of the film and substrate respectively, υ_f and υ_s are the film and substrate Poisson's ratios, t is the film thickness and h is the indent depth. The weighting factors, in parentheses, are exponential terms that incorporate the Poisson's ratio of each material and account for the lateral elastic interplay between the film and substrate. A principal feature of IIM is that the main constants are all elastic properties of the film and substrate, which are usually their bulk literature values. The model has shown to be adept at modelling the composite elastic response of a penetrating indenter obtained by the Oliver and Pharr method

(Oliver and Pharr, 1992) for numerous film/substrate composites (Chen et al., 2018; Liu et al., 2011a; Liu et al., 2011b; Sullivan et al., 2015; Sullivan and Prorok, 2015; Xu et al., 2018; Zhou and Prorok, 2010a; Zhou and Prorok, 2010b).

$$\frac{1}{E} = \frac{1}{E_f}\left(1 - e^{-v_s(t/h)}\right) \cdot \left(\frac{E_f}{E_s}\right)^{0.1} + \frac{1}{E_s}\left(e^{-v_f(t/h)}\right) \quad (2)$$

Two important aspects of IMM are (1) rearranging Equation 2 to decouple the film and substrate contributions and (2) taking advantage of the fact that the weighting factors in Equation 2 are actually specific types of hyperbolic functions. The first is accomplished by dividing both sides by the weighting factor on the film compliance $(1 - e^{-v_s(t/h)})$ as,

$$\frac{1}{E}\left[\frac{1}{(1-e^{-v_s(t/h)})}\right] = \frac{1}{E_f} \cdot \left(\frac{E_f}{E_s}\right)^{0.1} + \frac{1}{E_s}\left[\frac{(e^{-v_f(t/h)})}{(1-e^{-v_s(t/h)})}\right]. \quad (3)$$

The second involves a convenient property of hyperbolic functions in that they approach an asymptote that is easily approximated with a simple linear function. These were found to be 0.5 + h/t for the bracket on the left side and $1/2 + v_f/v_s + (h/t)/v_s$ for the bracket on the right (Batyuskov, 2001), see Equation 4. The result is a linear function with a slope of $1/(v_s E_s)$.

$$\frac{1}{E}\frac{1}{(0.5+h/t)} = \frac{1}{E_f} \cdot \left(\frac{E_f}{E_s}\right)^{0.1} + \frac{1}{E_s}\left(\frac{1}{2} - \frac{v_f}{v_s} + \frac{h/t}{v_s}\right). \quad (4)$$

The IMM procedure simply involves multiplying the composite modulus from the indenter by the film-side weighting factor to obtain the reduced modulus, left-side of Equation 3 or 4. As the indenter penetrates the film and approaches the film/substrate interface, where h/t = 1, the reduced modulus approaches its linear asymptote, whose slope is directly related to the substrate's elastic modulus. The film elastic modulus and Poisson's ratio are contained in the constant/intercept of the linear form in Equation 4 and do not influence the magnitude of the slope. Thus, by depositing a thin metallic film and confining the penetration only to the film, IIM can directly measure the elastic properties of a material in the absence of extreme deformation events/behavior.

The development of geologic-based deformation models depends on knowledge of the constituent material properties for validation and prediction accurately. IIM is an ideal technique for rapid determination of elastic properties for many geologic materials, which can more readily be investigated as a function of composition, structure, hydration, or other physical characteristic. The aim of this work is to demonstrate its ease of use and applicability to standard geologic materials as well as those whose elastic properties have been difficult to ascertain. Talc for example is considered one of the softest minerals as its hardness defines the lowest value on Mohs' Hardness scale (Gerberich et al., 2015; Mohs, 1925). However, this intrinsically weak behavior has resisted efforts to measure its true elastic properties, which have scarcely been reported on in the literature. Results of IIM will be presented on typical materials found in geologic settings as well as reliable measurements of elastic modulus challenging materials such as talc and galena.

Experimental Methodology

Sample Preparation

Ten geologic relevant materials were chosen for study; naturally occurring kyanite, feldspar orthoclase, dolomite, microcline, obsidian, galena, beryl calcite, quartz and talc (obtained from Scott Resources). These materials were chosen to demonstrate the indirect indentation method on minerals possessing a wide variety of material properties and deformation behavior. Table 1 lists the common literature values of their elastic moduli and Poisson's ratios. Here, citations were chosen that (1) represented the average of the reported elastic data and (2) used methods other than indentation to determine their values. Samples of each were mounted in epoxy and rough polished with sand paper and then fine polished with colloidal Al_2O_3 media suspensions to produce mirror-like finishes, typically less than 5 nm RMS roughness over 1 mm^2 area. X-ray diffraction was performed to confirm each material and determine the crystallographic orientation being tested for the single crystal samples. Chromium was chosen as the metallic film to absorb the inelastic damage from the penetrating indenter. It is ductile and has a Poisson's ratio of 0.21 (Samaonov, 1968). It is also easily deposited via sputter deposition (Sullivan and Prorok, 2015) and can wet a wide variety of materials to form a strong interface (Ohring, 2001). Films were deposited using a Denton Discovery 18 sputtering system with substrate rotation to ensure a uniform coating. Process parameters were set at a DC power of 200 W and an argon gas flow of 25 sccm (Liang and Prorok, 2007; Wang et al., 2007; Wang and Prorok, 2008). Chromium film deposition was performed on all samples simultaneously to ensure all minerals possessed films of consistent thickness and morphology. Film thickness was measured on film/mineral cross-sections with a JEOL 7000F scanning electron microscope (SEM). Indent images were also captured by the SEM using secondary electron imaging.

Table 1: Literature values of the elastic modulus and Poisson's ratios of the materials involved and their comparison with results from the indirect indentation method.

Material	Literature Values			Indirect Indentation Method
	E (GPa)	v	[ref]	E (GPa)
Chromium	190 ± 8	0.210	(Samaonov, 1968)	---
Kyanite (100)	227 ± 30	0.290	(Mikowski et al., 2008; Whitney et al., 2007)	228.6 ± 11
Feldspar Orthoclase (002)	89 ± 7	0.240	(Christensen, 1996; Whitney et al., 2007)	77.0 ± 2
Dolomite (polycrystalline)	53-85	0.200	(Grady et al., 1976; Viktorov et al., 2014)	93.6 ± 4
Microcline(polycrystalline)	69	0.245	(Christensen, 1996; Zhou et al., 2016)	73.8 ± 3
Obsidian (amorphous)	65 ± 2	0.185	(Bass, 1995; Husien, 2010)	66.8 ± 2
Galena (002)	--	0.270	(Gercek, 2007)	58.2 ± 2
Beryl (amorphous)	212	0.039	(Yeganehhaeri and Weidner, 1989; Yoon and Newnham, 1973)	214.2 ± 7
Calcite (104)	69 ± 2	0.322	(Fiquet et al., 1994; Redfern and Angel, 1999)	66.3 ± 2
Quartz	107 ± 3	0.079	(Bass, 1995; Gercek, 2007)	97.4 ± 4
Talc	--	0.268	(Bailey and Holloway, 2000)	218.7 ± 6

This is the peer-reviewed, final accepted version for American Mineralogist, published by the Mineralogical Society of America.
The published version is subject to change. Cite as Authors (Year) Title. American Mineralogist, in press.
DOI: https://doi.org/10.2138/am-2021-7455. http://www.minsocam.org/

Mechanical Testing

The mechanical response of the samples was interrogated with an MTS Nanoindenter XP with a Berkovich diamond tip operated under continuous stiffness mode (CSM). Indents were performed directly on the polished mineral samples and indirectly on the Cr/mineral composites. Here, the elastic modulus was measured as a function of penetration depth. The CSM testing frequency was set at 45Hz with a harmonic displacement target of 2nm and was conducted under a 0.05 nm/s thermal drift rate threshold. Each sample was indented in a 5 × 5 array with a 100 μm spacing between indents. The elastic modulus was determined from the unloading stiffness (Oliver and Pharr, 1992). The mean elastic modulus of the 25 indents on each sample was reported as a function of indenter depth with error bars representing one standard deviation. Micrographs of indents were acquired by the SEM.

Data Analysis

The Indirect Indentation Method (Chen et al., 2018) was employed to determine the elastic properties of the minerals. The first step was to multiply the mean composite elastic modulus obtained from the nanoindenter by the film-side weighting factor, as per the left-side of Equation 3. Here, the mineral's literature Poisson's ratio (v_s) from Table 1 was used. In fact, any value can be assumed with negligible effects as long as it is within the normal range of 0.0 to 0.5. This results in a plot of the reduced modulus as a function of the normalized displacement (h/t), shown later. The slope near the film/mineral interface was determined in the h/t range from 0.6 to 1.0 (Chen et al., 2018) and was equated to $1/(E_s v_s)$, as per the right-side of Equation 4. The elastic modulus of the mineral (E_s) was then calculated using the Poisson's ratio (v_s) assumed when obtaining the reduced modulus. The instantaneous slope of each reduced modulus data point was then used to calculate the indirect elastic modulus as a function of h/t.

Results and Discussion

Direct Indentation

The materials kyanite (100) and feldspar orthoclase were chosen to demonstrate the applicability of the indirect indentation method to geologic materials. Both materials were indented to a depth of 1 μm, and the measured elastic modulus was plotted as a function of displacement into the surface, see Figures 1 (a) and (b). Both material curves begin at values higher than their literature values, denoted by dashed lines and listed in Table 1, and then decrease as the indenter penetrates the materials. The high values at low displacements are a result of the indenter geometry. Although the Berkovich tip has a three sided pyramid geometry, the tip is actually spherical with a radius of 30 to 50 nm. Thus, the first 50 nm or so of contact has more projected contact area than the pyramidal geometry, artificially inflating the modulus values. Neither curve in Figure 1 reaches a point where the modulus remains consistent enough to estimate a value. In fact, the feldspar modulus drops well below its literature value for the majority of the penetration depth. The behavior of both materials indicate that inelastic processes are likely consuming energy that would normally be stored elastically and recovered during unloading.

The load-displacement curves for directly indenting both materials can help explain the varying modulus results, see Figures 2 (a) and (b). As the indenter penetrates both samples, each material resists and absorbs the applied load through elastic and inelastic deformation mechanisms that vary based on the material and its microstructure. The kyanite curve reveals three discrete events where the displacement into the surface increased rapidly, denoted by arrows. These can be explained by large-scale cleavage and sliding of its lamellar structure (Boland et al., 1977; Doukhan and Christie, 1982; Doukhan and Paquet, 1982; Lefebvre, 1982; Lefebvre and Menard, 1981; Raleigh, 1965). An electron micrograph of a direct indent made on kyanite is shown in Figure 3(a). Here, the triangular residual indent is seen with lamella sliding occurring on (100) where the face of the indenter tip contacts the material and cleavage along the (010) plane occurring where its edge makes contact, labelled as (1) and (2) respectively. The feldspar sample did not exhibit discreet events in its load displacement response, Figure 2(b). However, an electron micrograph of a direct indent, Figure 3(b), reveals that the material experienced significant cracking at the edges of the indenter tip, (3), that continually increased as it penetrated. The large displacement events in the kyanite and the cracking in the feldspar are inelastic defects that consume energy that would normally be stored elastically in their absence. Thus, their irreversible formation influences the unloading stiffness, and thereby elastic modulus, through reduced elastic recovery from the sample. Directly indenting these materials to determine elastic response was hindered by the presence and evolution of these inelastic deformation processes.

Indirect Indentation

A 940 nm thick chromium film was deposited on the samples to shield the materials from the inelastic deformation processes caused by the penetrating indenter. The samples were indented and imaged by the SEM, Figures 3 (c) and (d), and suggest the chromium film was successful in absorbing the majority if inelastic deformation for both materials. Figures 4 (a) and (b) show the elastic modulus results from the nanoindenter for the Cr/mineral composites. Here the results are plotted as h/t to reflect how far the indenter has penetrated into the film, which is the base form of the hyperbolic determination analysis. As the film thickness was 940 nm, this scale is comparable to the results in Figure 1, which was plotted as h for an indent depth of 1000 nm. The results from both materials show improved progression to consistent elastic modulus values with increasing h/t over the direct

DOI: https://doi.org/10.2138/am-2021-7455. http://www.minsocam.org/

indentation results. The kyanite sample appears to level off after an h/t of 0.5 is reached while the feldspar sample has not yet reached a consistent value. The chromium/Kyanite value is very similar to its literature value of 227 GPa (Mikowski et al., 2008; Whitney et al., 2007), denoted by the dashed line in Figure 4. However, this is only a convenient happenstance as the chromium film possesses a very similar elastic modulus and Poisson's ratio as kyanite, see Table 1. Thus, the two materials, are elastically similar.

In order to begin the hyperbolic analysis of the indirect indentation model, the reduced modulus was determined for both materials. This was accomplished by multiplying the mean composite elastic modulus obtained from the nanoindenter by the film-side weighting factor, as per the left-side of Equation 3. A Poisson's ratio of 0.24 and 0.29 was assumed for kyanite and feldspar respectively, see Table 1. Figures 5 (a) and (b) plot the reduced modulus as a function of h/t for both materials. After penetrating an h/t of 0.4 into the film, both materials exhibited a strong linear behavior, denoted by the dashed lines. The slope of these lines was determined by liner regression for all points in the h/t range of 0.6 to 1.0 as per the method development (Chen et al., 2018). Slopes of 0.016833 GPa^{-1} and 0.044482 GPa^{-1} were found for the kyanite and feldspar samples respectively. Using the assumed Poisson's ratios of each material, the elastic modulus of the kyanite was calculated to be 228 ±11 GPa and 77 ±2 GPa for feldspar, which match rather well with the literature values in Table 1. The indirect hyperbolic analysis was applied to each individual data point through the instantaneous slope. This yielded a plot of the indirect measured elastic modulus of the mineral as a function of penetration depth into the film (h/t), see Figures 6 (a) and (b). When both materials reach an h/t of 0.6 or higher, their measured elastic modulus reaches a consistent value numerically similar to their literature value, the dashed lines. This method was repeated for the other geologic relevant materials listed in Table 1 with results plotted in Figure 7 (a). Here, the reduced modulus for the remaining materials is plotted in Figure 7 (a) and their indirect measured modulus in Figure 7 (b). All of the materials attained a strong linear relationship in the method's h/t range of 0.6 to 1.0, enabling their elastic modulus to be determined, see Table 1. The indirect indentation results for all of the materials matched well with the average literature values but also varied somewhat. These differences likely reflect variations in compositions, microstructure and other characteristics that play a role in mechanical behavior. All materials also exhibited very stable values of indirect modulus in the same h/t range. In fact, all materials, with the exception of Galina, achieved stable values around an h/t value of 0.4, which is less than half the film thickness. Finally, the indirect indentation method was adept at obtaining very stable elastic moduli for Galena and Talc. These two materials have been historically difficult to measure due to their wide variability in deformation based on impurity content, hydration, pressure and unusual deformation (Stixrude, 2002). In fact, the indirect indentation method would be an ideal method to investigate and discern any variation in mineral elastic behavior as a function of composition, formation conditions, and other physical differences.

Implications

This work has demonstrated that indirect indentation method, which employs a metallic film to absorb damage from the penetrating indenter, was adept at extracting elastic moduli from several geologically relevant rocks and minerals. Measured values of elastic modulus matched rather well with the literature for all materials tested. Tested materials included natural rocks and minerals that possessed unusual deformation behavior including brittle materials and materials with complex architectures and deformation behavior. In addition to absorbing the highly localized deformation from the indenter, the metallic film was successful at containing the sample deformation to within the elastic regime, enabling it to be directly measured with IIM. Furthermore, IIM was also successful in establishing the elastic modulus of talc and galena, whose elastic behaviors have been difficult to ascertain. This new method will enable geological scientists and engineers to rapidly determine the elastic behavior of most rocks or minerals in a simple manner with a robust statistical response. It will also facilitate investigations of their elastic properties as a function of composition, structure, hydration, or other physical characteristic. This will undoubtedly impact the development of geologic-based deformation models through knowledge of the constituent material properties for validation and prediction accurately.

References

Angel, R.J., Jackson, J.M., Reichmann, H.J., and Speziale, S. (2009) Elasticity measurements on minerals: a review. European Journal of Mineralogy, 21(3), 525-550.

Atkinson, B.K. (1976) The temperature- and strain rate-dependent mechanical behavior of a polycrystalline galena ore. Economic Geology, 71(2), 513-525.

Bailey, E., and Holloway, J.R. (2000) Experimental determination of elastic properties of talc to 800 degrees C, 0.5 GPa; calculations of the effect on hydrated peridotite, and implications for cold subduction zones. Earth and Planetary Science Letters, 183(3-4), 487-498.

Bass, J.D. (1995) Elasticity of minerals, glasses and melts. In T.J. Ahrens, Ed. Mineral physics and crystallography: a handbook of physical constants. American Geophysical Union, Washington DC.

Batyuskov, V.I. (2001) Hyperbolic functions. In M. Hazewinkel, Ed. Encyclopedia of Mathematics, 4, p. 496. Springer.

Blackman, D.K., Wenk, H.R., and Kendall, J.M. (2002) Seismic anisotropy of the upper mantle 1. Factors that affect mineral texture and effective elastic properties. Geochemistry, Geophysics, Geosystems, 3(9), 1-24.

Boland, J.N., Hobbs, B.E., and McLaren, A.C. (1977) Defect structure in natural and experimentally deformed cyanite. Physica Status Solidi a-Applied Research, 39(2), 631-641.

Chen, Y., Sullivan, M., Zhang, A.Q., and Prorok, B.C. (2018) A new method to extract elastic modulus of brittle materials from Berkovich indentation. Journal of the European Ceramic Society, 38(1), 349-353.

Christensen, N.I. (1996) Poisson's ratio and crustal seismology. Journal of Geophysical Research-Solid Earth, 101(B2), 3139-3156.

Constantinides, G., Ravi Chandran, K.S., Ulm, F.J., and Van Vliet, K.J. (2006) Grid indentation analysis of composite microstructure and mechanics: Principles and validation. Materials Science and Engineering: A, 430(1), 189-202.

Doerner, M.F., and Nix, W.D. (1986) A method for interpreting the data from depth-sensing indentation instruments. Journal of Materials Research, 1(4), 601.

Doukhan, J.C., and Christie, J.M. (1982) Plastid-deformation of sillimanite AL2SIO5 single-crystals under cinfining pressure and TEM investigation of the induced defect structure. Bulletin De Mineralogie, 105(6), 583-589.

Doukhan, J.C., and Paquet, J. (1982) Plastid-deformation of andalusite single-crystal AL2SIO5. Bulletin De Mineralogie, 105(2), 170-175.

Ersoy, A., and Waller, M.D. (1995) Textural characterisation of rocks. Engineering Geology, 39(3), 123-136.

Fiquet, G., Guyot, F., and Itie, J.P. (1994) High-pressure X-ray diffraction study of carbonates - MGCO3, CAMG(CO3)2, AND CACO3. American Mineralogist, 79(1-2), 15-23.

Gerberich, W.W., Ballarini, R., Hintsala, E.D., Mishra, M., Molinari, J.F., and Szlufarska, I. (2015) Toward Demystifying the Mohs Hardness Scale. Journal of the American Ceramic Society, 98(9), 2681-2688.

Gercek, H. (2007) Poisson's ratio values for rocks. International Journal of Rock Mechanics and Mining Sciences, 44(1), 1-13.

Grady, D.E., Murri, W.J., and Mahrer, K.D. (1976) Shock compression of dolomite. Journal of Geophysical Research, 81(5), 889-893.

Hintsala, E.D., Hangen, U., and Stauffer, D.D. (2018) High-Throughput Nanoindentation for Statistical and Spatial Property Determination. JOM - The Journal of The Minerals, Metals & Materials Society (TMS), 70(4), 494-503.

Husien, M.S. (2010) Fracture Behavior and Mechanical Characterization of Obsidian: Naturally Occuring Glass. Mechanical Engineering, Master of Science, p. 40. Oklahoma State University.

King Hubbert, M. (1951) Mechanical Basis for Certain Familiar Geologic Structures. GSA Bulletin, 62(4), 355-372.

King, R.B. (1987) Elastic analysis of some punch problems for a layered medium. International Journal of Solids and Structures, 23(12), 1657.

Lefebvre, A. (1982) Transmission electron-microscopy of andalusite single-crystals indented at roon-temperature. Bulletin De Mineralogie, 105(4), 347-350.

Lefebvre, A., and Menard, D. (1981) Stacking-faults and twins in kyanite, AL2SIO5. Acta Crystallographica Section A, 37(JAN), 80-84.

Liang, C., and Prorok, B.C. (2007) Measuring the thin film elastic modulus with a magnetostrictive sensor. Journal of Micromechanics and Microengineering, 17(4), 709-716.

Liu, D., Zhou, B., Yoon, S.H., Kim, S.B., Ahn, H., Prorok, B.C., Kim, S.H., and Kim, D.J. (2011a) Determination of the True Young's Modulus of Pb(Zr0.52Ti0.48)O-3 Films by Nanoindentation: Effects of Film Orientation and Substrate. Journal of the American Ceramic Society, 94(11), 3698-3701.

Liu, D., Zhou, B., Yoon, S.H., Wikle, H.C., Wang, Y.Q., Park, M., Prorok, B.C., and Kim, D.J. (2011b) Effects of the structural layer in MEMS substrates on mechanical and electrical properties of Pb(Zr0.52Ti0.48)O-3 films. Ceramics International, 37(7), 2821-2828.

Meyers, M.A., and Chawla, K.K. (2009) Mechanical Behavior of Materials. Cambridge University Press, New York.

Mikowski, A., Soares, P., Wypych, F., Gardolinski, J., and Lepienski, C.M. (2007) Mechanical properties of kaolinite 'macro-crystals'. Philosophical Magazine, 87(29), 4445-4459.

Mikowski, A., Soares, P., Wypych, F., and Lepienski, C.M. (2008) Fracture toughness, hardness, and elastic modulus of kyanite investigated by a depth-sensing indentation technique. American Mineralogist, 93(5-6), 844-852.

Mohs, F. (1925) Treatise on Mineralogy. Caledonian Mercury Press, Edinburgh.

Na, S., Sun, W., Ingraham, M.D., and Yoon, H. (2017) Effects of spatial heterogeneity and material anisotropy on the fracture pattern and macroscopic effective toughness of

DOI: https://doi.org/10.2138/am-2021-7455. http://www.minsocam.org/

Mancos Shale in Brazilian tests. Journal of Geophysical Research: Solid Earth, 122(8), 6202-6230.

Ohring, M. (2001) Materials Science of Thin Films. Academic Press.

Oliver, W.C., and Pharr, G.M. (1992) An improved technique for determining hardness and elastic modulud using load and displacement sensing indentation experiments. Journal of Materials Research, 7(6), 1564.

- (2004) Measurement of hardness and elastic modulus by instrumented indentation: Advances in understanding and refinements to methodology. Journal of Materials Research, 19(1), 3-20.

Pharr, G.M., and Bolshakov, A. (2002) Understanding nanoindentation unloading curves. Journal of Materials Research, 17(10), 2660.

Pharr, G.M., Strader, J.H., and Oliver, W.C. (2009) Critical issues in making small-depth mechanical property measurements by nanoindentation with continuous stiffness measurement. Journal of Materials Research, 24(3), 653-666.

Raisanen, M. (2004) Relationships between texture and mechanical properties of hybrid rocks from the Jaala–Iitti complex, southeastern Finland. Engineering Geology, 74, 197-211.

Raleigh, C.B. (1965) Glide mechanisms in experimentally deformed minerals. Science, 150(3697), 739-741.

Randall, N.X., Vandamme, M., and Ulm, F.-J. (2009) Nanoindentation analysis as a two-dimensional tool for mapping the mechanical properties of complex surfaces. Journal of Materials Research, 24(3), 679-690.

Redfern, S.A.T., and Angel, R.J. (1999) High-pressure behaviour and equation of state of calcite, CaCO3. Contributions to Mineralogy and Petrology, 134(1), 102-106.

Reuss, A. (1929) Berechnung der Fließgrenze von Mischkristallen auf Grund der Plastizitätsbedingung für Einkristalle. ZAMM - Journal of Applied Mathematics and Mechanics / Zeitschrift für Angewandte Mathematik und Mechanik, 9(1), 49-58.

Riecker, R.E. (1984) Rock mechanicsRock mechanics. In C.W. Finkl, Ed. Applied Geology, p. 482-489. Springer US, Boston, MA.

Samaonov, G.V. (1968) Handbook of the Physicochemical Properties of the Elements. Springer US.

Stixrude, L. (2002) Talc under tension and compression: Spinodal instability, elasticity, and structure. Journal of Geophysical Research-Solid Earth, 107(B12).

Sullivan, M., Chen, Y., and Prorok, B.C. (2015) New Strengthening Mechansims of Nacre in the Abalone Shell. International Journal of Experimental and Computational Biomechanics, 3(3), 236-249.

Sullivan, M., and Prorok, B.C. (2015) Evaluating indent pile-up with metallic films on ceramic-like substrates. Journal of Materials Research, 30(13), 2046-2054.

Sun, W., Wang, L., and Wang, Y. (2017) Mechanical properties of rock materials with related to mineralogical characteristics and grain size through experimental investigation: a comprehensive review. Frontiers of Structural and Civil Engineering, 1-7.

Tandon, R.S., and Gupta, V. (2013) The control of mineral constituents and textural characteristics on the petrophysical & mechanical (PM) properties of different rocks of the Himalaya. Engineering Geology, 153, 125-143.

Viktorov, S.D., Golovin, Y.I., Kochanov, A.N., Tyurin, A.I., Shuklinov, A.V., Shuvarin, I.A., and Pirozhkova, T.S. (2014) Micro- and nano-indentation approach to strength and deformation characteristics of minerals. Journal of Mining Science, 50(4), 652-659.

Wang, L., Liang, C., and Prorok, B.C. (2007) A comparison of testing methods in assessing the elastic properties of sputter-deposited gold films. Thin Solid Films, 515(20-21), 7911.

Wang, L., and Prorok, B.C. (2008) Characterization of the strain rate dependent behavior of nanocrystalline gold films. Journal of Materials Research, 23(1), 55-65.

Whitney, D.L., Broz, M., and Cook, R.F. (2007) Hardness, toughness, and modulus of some common metamorphic minerals. American Mineralogist, 92(2-3), 281-288.

Xu, Y., Chen, Y., Zhang, A.Q., Jackson, R.L., and Prorok, B.C. (2018) A New Method for the Measurement of Real Area of Contact by the Adhesive Transfer of Thin Au film. Tribology Letters, 66(1).

Yeganehhaeri, A., and Weidner, D.J. (1989) Elasticity of a beryllium silicate (Phenacite-BE2SIO4). Physics and Chemistry of Minerals, 16(4), 360-364.

Yoon, H.S., and Newnham, R.E. (1973) Elastic properties of beryl. Acta Crystallographica Section A, A 29(SEP1), 507-509.

Zhou, B., and Prorok, B.C. (2010a) A Discontinuous Elastic Interface Transfer Model of Thin Film Nanoindentation. Experimental Mechanics, 50(6), 793-801.

-. (2010b) A new paradigm in thin film indentation. Journal of Materials Research, 25(9), 1671-1678.

Zhou, H., Liu, H.T., Hu, D.W., Yang, F.J., Lu, J.J., and Zhang, F. (2016) Anisotropies in Mechanical Behaviour, Thermal Expansion and P-Wave Velocity of Sandstone with Bedding Planes. Rock Mechanics and Rock Engineering, 49(11), 4497-4504.

Figure Captions

Fig. 1. Direct indentation results of Kyanite (a) and Feldspar (b) showing the elastic modulus versus displacement into the surface. The dashed line represents the literature values of each material given in Table 1.

Fig. 2. Load on sample versus displacement into surface for directly indenting Kyanite (a) and feldspar (b). The arrows highlight several pop-in events during penetration.

Fig 3. Scanning electron micrographs in secondary electron mode of residual indents on the kyanite, direct indent (a) and indirect indent (b), and feldspar, direct indent (c) and indirect indent (d).

Fig. 4. The indirect indentation results of Kyanite (a), left, and Feldspar (b) showing the elastic modulus versus displacement into the surface. The dashed line represents the literature value of each material from Table 1.

Fig. 5. The calculated reduced modulus results of kyanite (a) and Feldspar (b). The dashed line represents the linear regression of reduced modulus from 0.6 to 1.0 h/t.

Fig. 6. The calculated indirect substrate modulus results of kyanite (a) and Feldspar (b). The dashed line represents the literature value for each material given in Table 1.

Fig. 7. The calculated reduced modulus (a) and indirect substrate modulus results (b) for the other geological materials tested.

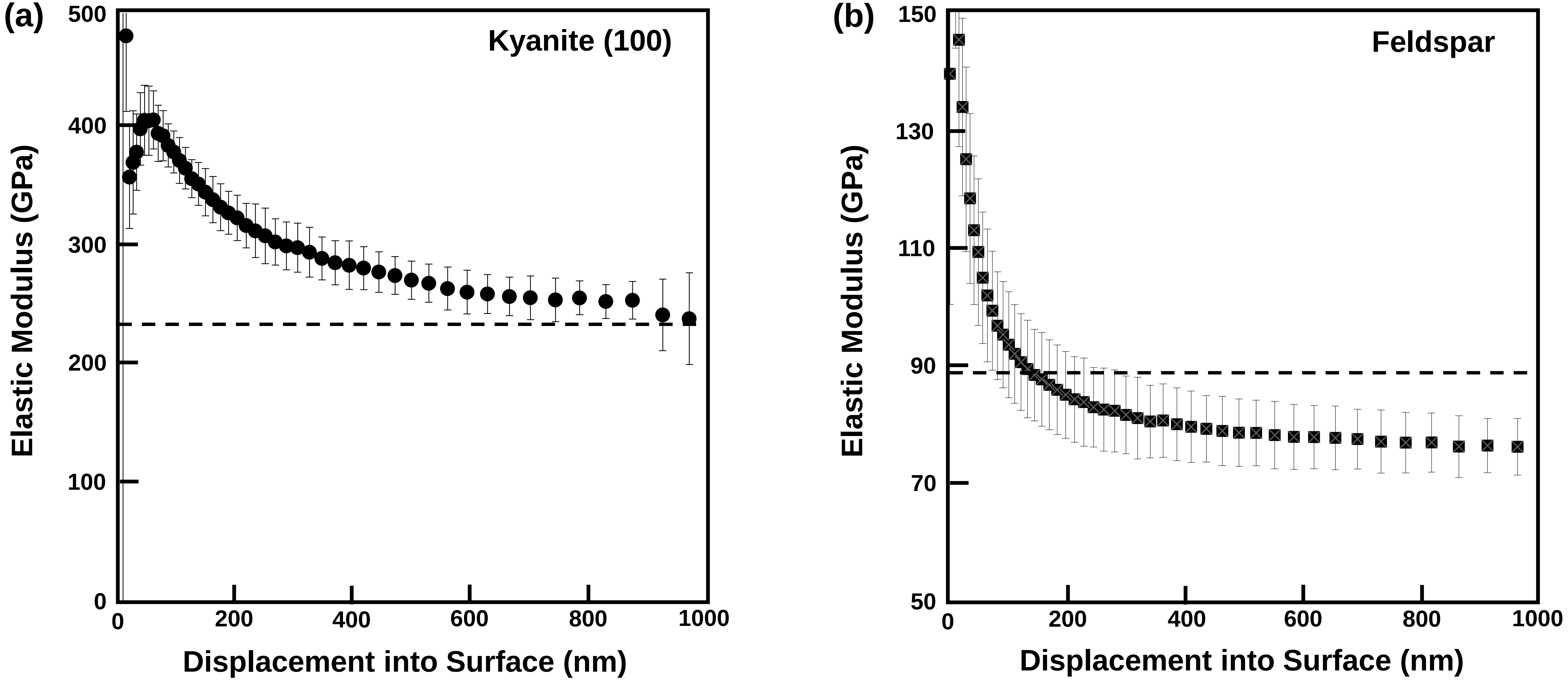
(a)
Kyanite (100)
Elastic Modulus (GPa)
500
400
300
200
100
0
0
200
400
600
800
1000
Displacement into Surface (nm)
(b)
Feldspar
Elastic Modulus (GPa)
150
130
110
90
70
50
0
200
400
600
800
1000
Displacement into Surface (nm)

Figure 1

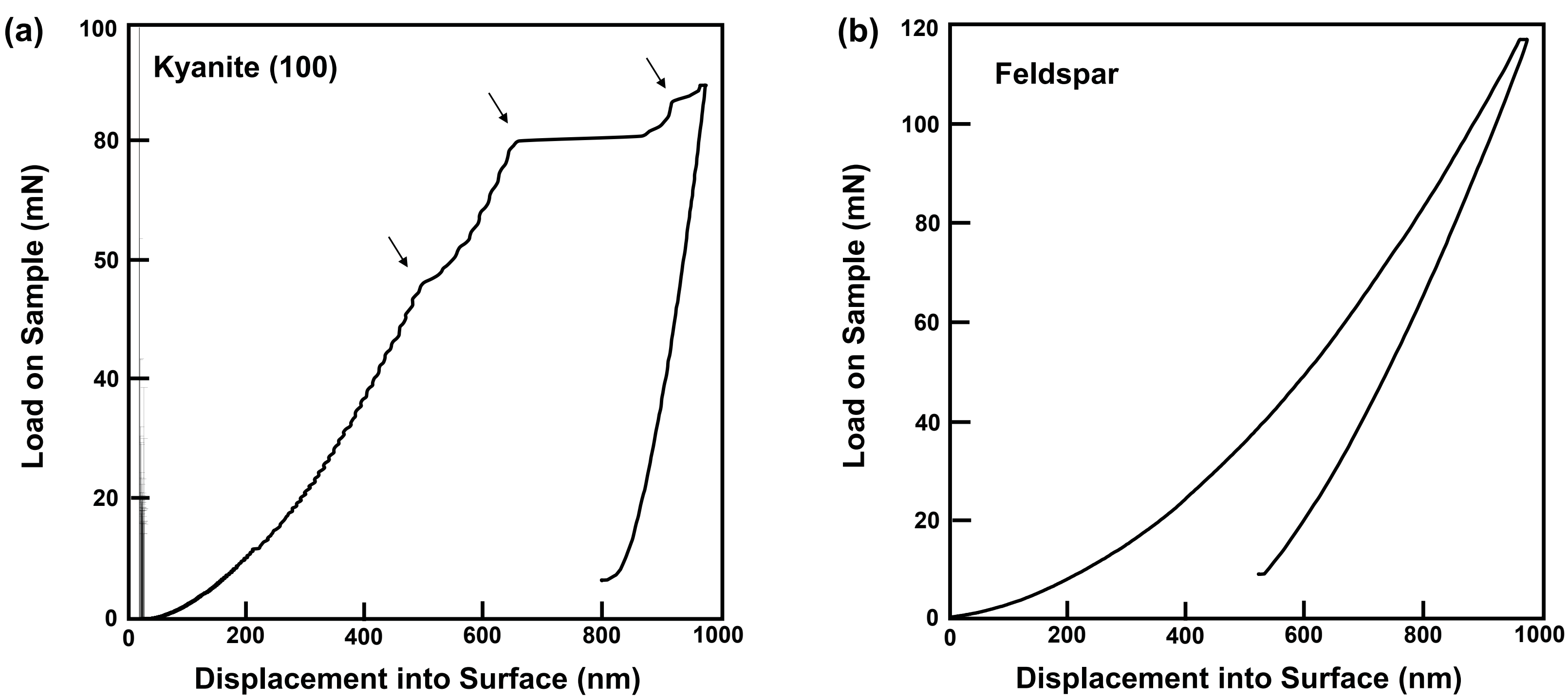

(a)
Kyanite (100)
Load on Sample (mN)
Displacement into Surface (nm)
0
20
40
50
80
100
0
200
400
600
800
1000
(b)
Feldspar
Load on Sample (mN)
Displacement into Surface (nm)
0
20
40
60
80
100
120
0
200
400
600
800
1000

Figure 2

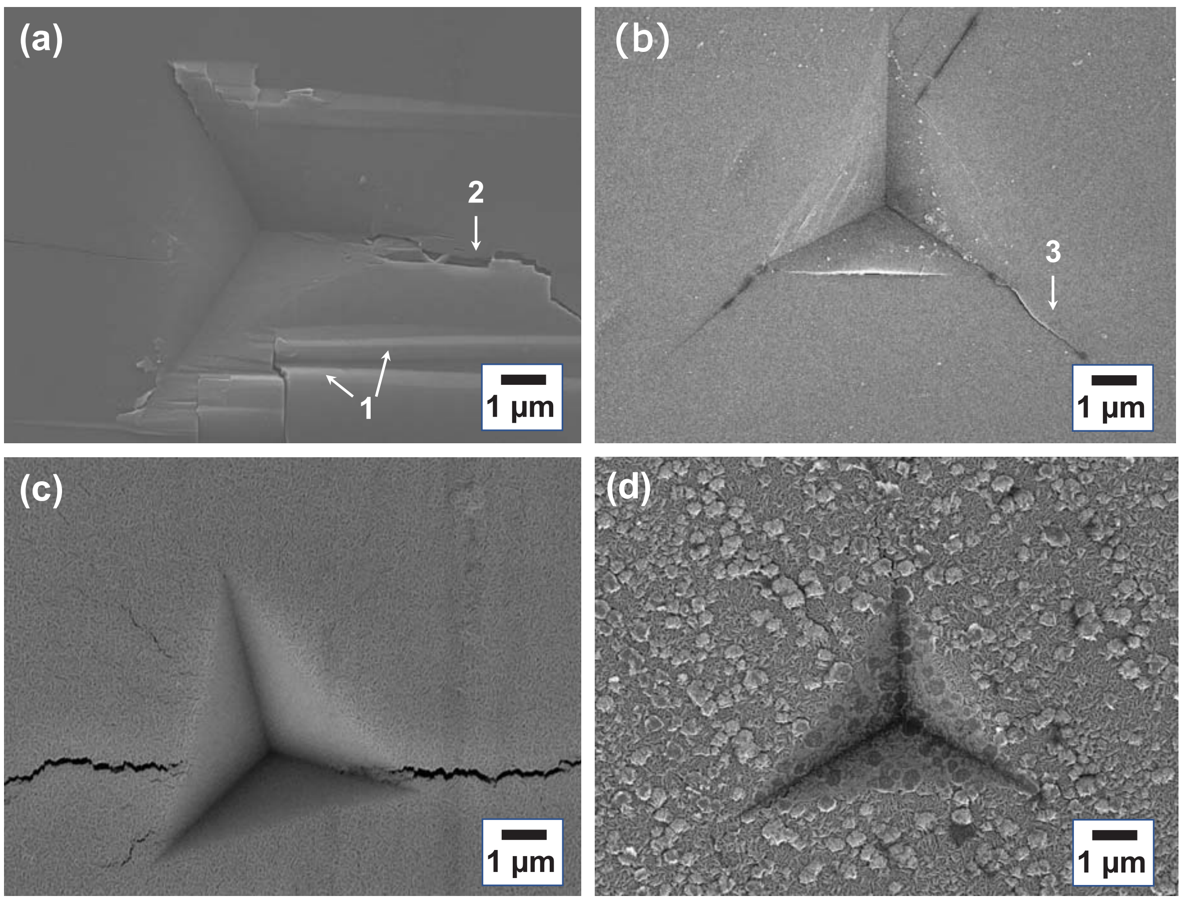

Figure 3

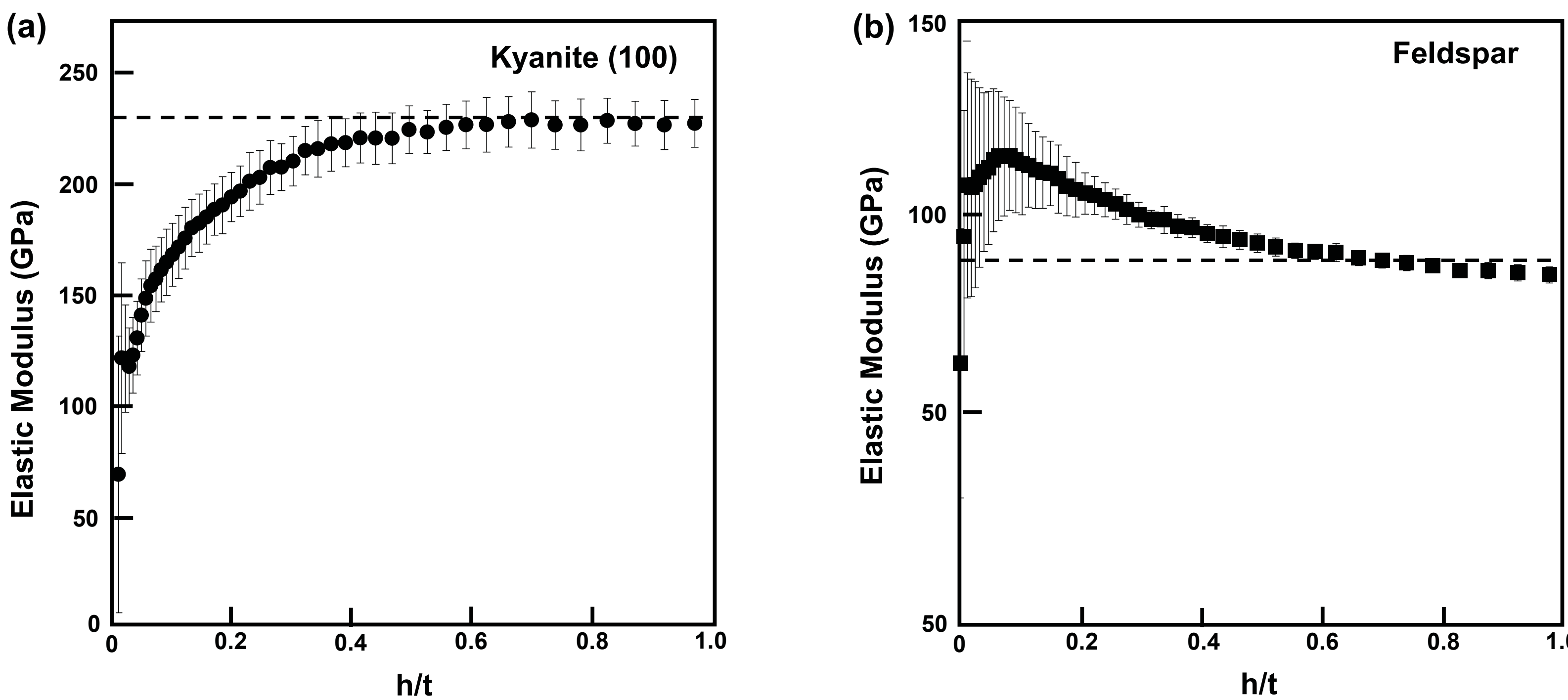
(a)
Kyanite (100)
Elastic Modulus (GPa)
h/t
0
50
100
150
200
250
0.2
0.4
0.6
0.8
1.0
(b)
Feldspar
Elastic Modulus (GPa)
h/t
50
100
150
0.2
0.4
0.6
0.8
1.0

Figure 4

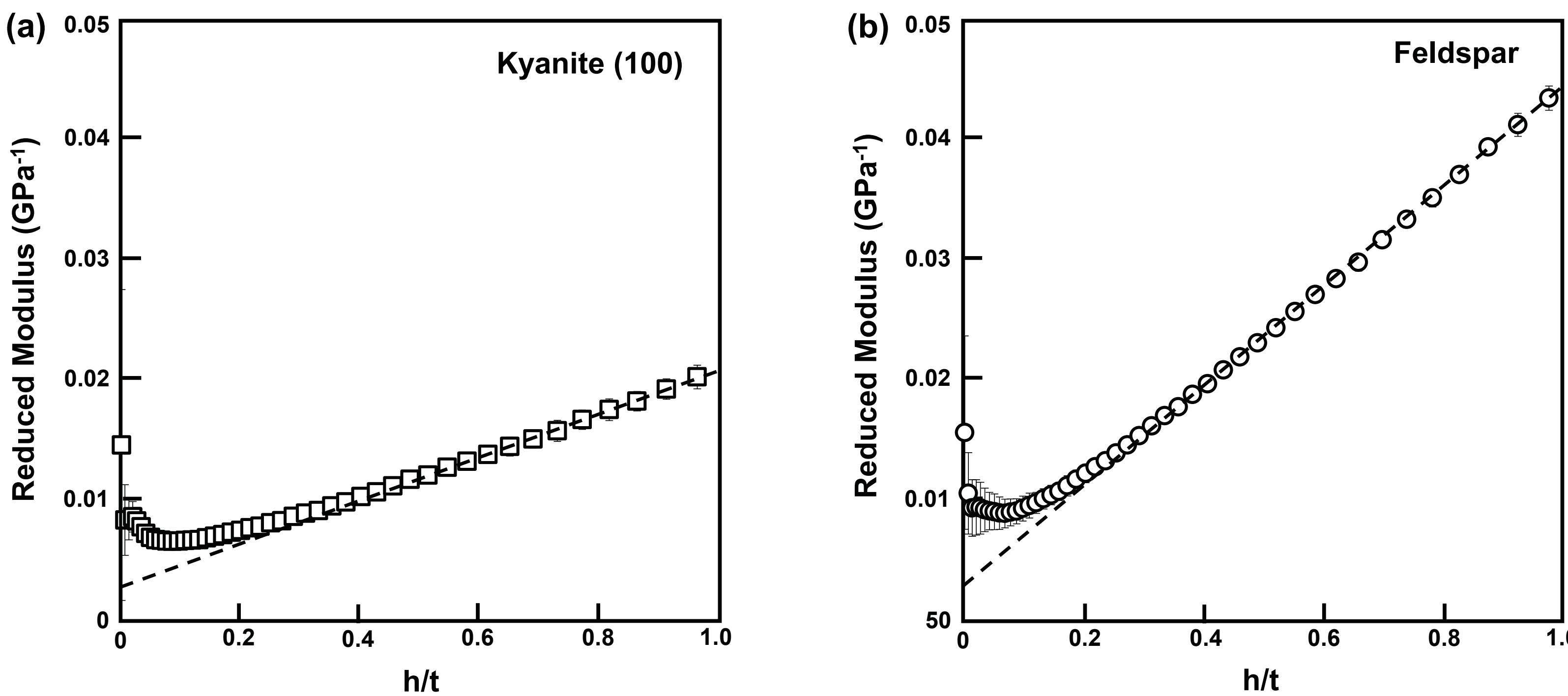
(a)
Kyanite (100)
Reduced Modulus (GPa-1)
0.05
0.04
0.03
0.02
0.01
0
0
0.2
0.4
0.6
0.8
1.0
h/t
(b)
Feldspar
Reduced Modulus (GPa-1)
0.05
0.04
0.03
0.02
0.01
50
0
0.2
0.4
0.6
0.8
1.0
h/t

Figure 5

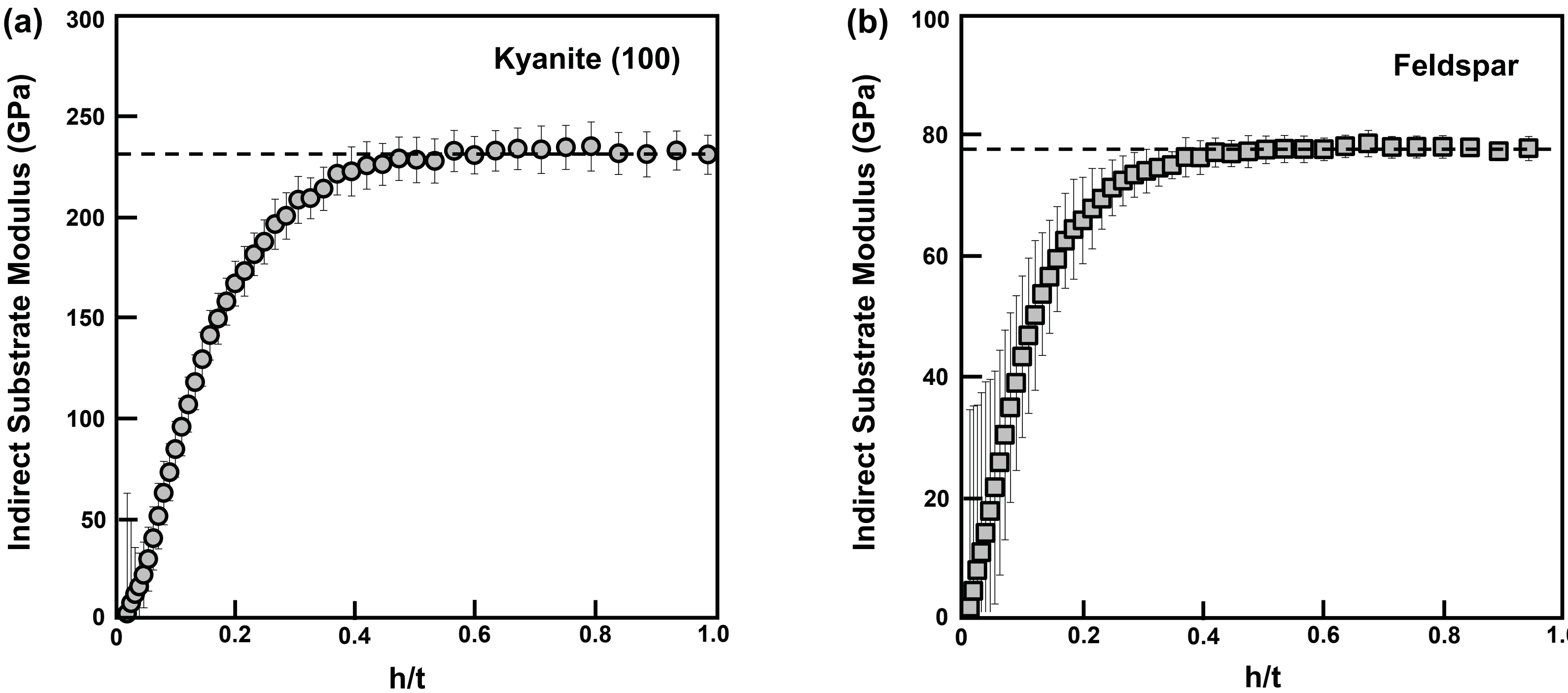

(a)
Kyanite (100)
Indirect Substrate Modulus (GPa)
300
250
200
150
100
50
0
0
0.2
0.4
0.6
0.8
1.0
h/t
(b)
Feldspar
Indirect Substrate Modulus (GPa)
100
80
60
40
20
0
0
0.2
0.4
0.6
0.8
1.0
h/t

Figure 6

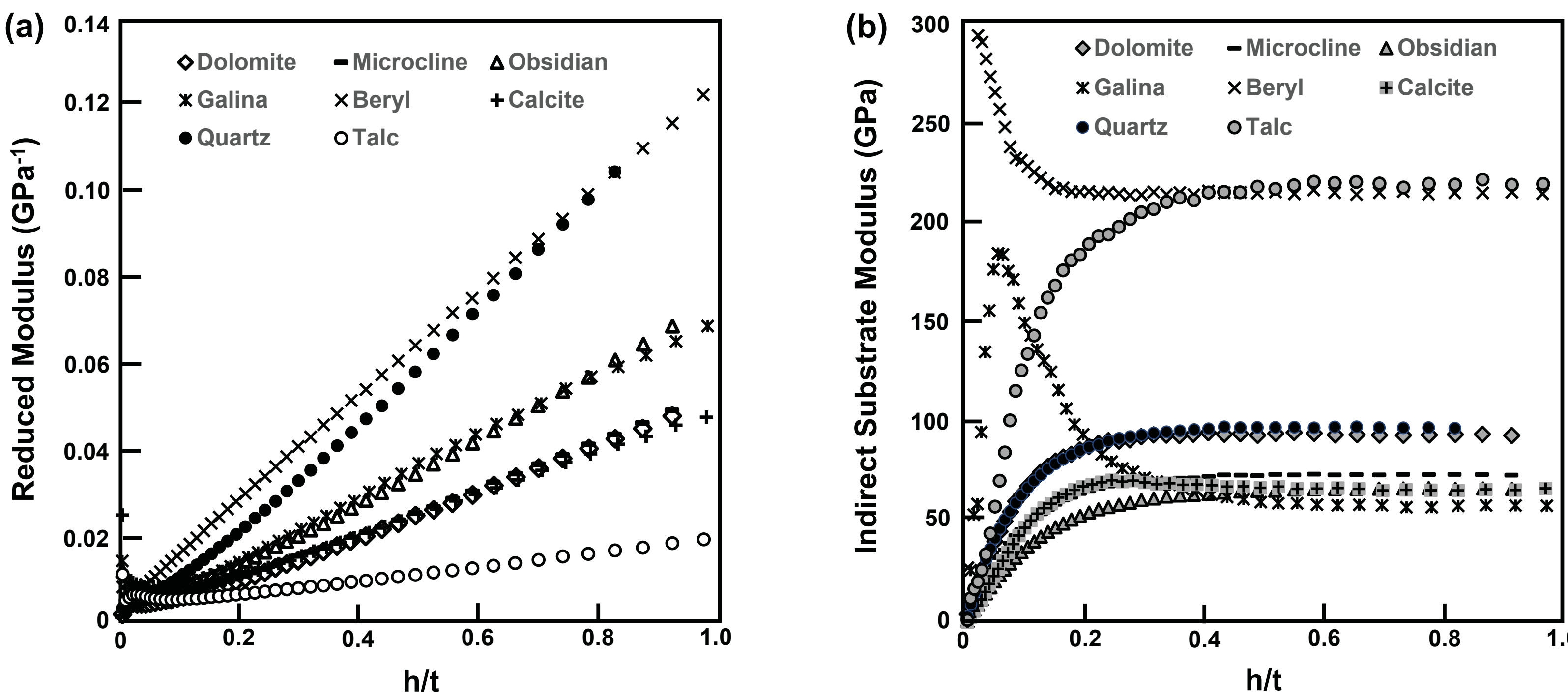
(a)
Dolomite
Microcline
Obsidian
Galina
Beryl
Calcite
Quartz
Talc
Reduced Modulus (GPa-1)
h/t
0.14
0.12
0.10
0.08
0.06
0.04
0.02
0
0
0.2
0.4
0.6
0.8
1.0
(b)
Dolomite
Microcline
Obsidian
Galina
Beryl
Calcite
Quartz
Talc
Indirect Substrate Modulus (GPa)
h/t
300
250
200
150
100
50
0
0
0.2
0.4
0.6
0.8
1.0

Figure 7